Frontiers of Information Technology & Electronic Engineering
www.jzus.zju.edu.cn; engineering.cae.cn; www.springerlink.com
ISSN 2095-9184 (print); ISSN 2095-9230 (online)
E-mail: jzus@zju.edu.cn

Event-triggered adaptive finite-time control for nonlinear systems under asymmetric time-varying state constraints*

Yan WEI[1], Jun LUO[2], Huaicheng YAN[3], Yueying WANG[†‡2]

[1]*School of Aeronautics and Astronautics, Shanghai Jiao Tong University, Shanghai 200240, China*

[2]*School of Mechatronic Engineering and Automation, Shanghai University, Shanghai 200444, China*

[3]*School of Information Science and Engineering, East China University of Science and Technology, Shanghai 200237, China*

[†]E-mail: wyy676@126.com

Received Dec. 11, 2020; Revision accepted Mar. 22, 2021; Crosschecked Sept. 2, 2021; Published online Nov. 3, 2021

Abstract: This paper investigates the issue of event-triggered adaptive finite-time state-constrained control for multi-input multi-output uncertain nonlinear systems. To prevent asymmetric time-varying state constraints from being violated, a tan-type nonlinear mapping is established to transform the considered system into an equivalent "non-constrained" system. By employing a smooth switch function in the virtual control signals, the singularity in the traditional finite-time dynamic surface control can be avoided. Fuzzy logic systems are used to compensate for the unknown functions. A suitable event-triggering rule is introduced to determine when to transmit the control laws. Through Lyapunov analysis, the closed-loop system is proved to be semi-globally practical finite-time stable, and the state constraints are never violated. Simulations are provided to evaluate the effectiveness of the proposed approach.

Key words: Event-triggered control; Nonlinear mapping; Adaptive fuzzy control; Finite-time; State constraints
https://doi.org/10.1631/FITEE.2000692 **CLC number:** TP13

1 Introduction

In recent years, some meaningful control technologies have been studied for a class of uncertain nonlinear systems. As an effective control method, backstepping control technology has been investigated and applied in uncertain nonlinear systems. To avoid the issue of "complexity explosion," dynamic surface control (DSC) (Swaroop et al., 2000) and command filter backstepping (Dong et al., 2012) have been proposed. Fuzzy logic systems (FLSs) (Yu et al., 2015; Tian et al., 2016) or neural networks (NNs) (Ge and Wang, 2004; Wang M et al., 2010) are usually combined with adaptive backstepping control technology to compensate for the unknown smooth functions.

Note that output/state constraints often occur in practical systems. The transgression of output/state constraints may decrease system performance or even cause danger. Considering the output/state constraints, barrier Lyapunov function (BLF) based control approaches have been proposed by Tee et al. (2009). Since then, many kinds of BLFs have been presented, such as log-type BLFs (Li GJ, 2017; Wei et al., 2019), tan-type BLFs (Jin, 2016), and integral BLFs (iBLFs) (Tee and Ge, 2012;

‡ Corresponding author

* Project supported by the National Natural Science Foundation of China (Nos. 61973204 and 61703275)

ORCID: Yan WEI, https://orcid.org/0000-0002-9818-8034; Yueying WANG, https://orcid.org/0000-0001-9737-6765

Wei et al., 2020b). When using log-type BLFs or tan-type BLFs, the output/state constraints should be transformed on error constraints, which leads to the initial state selection tending to be conservative. When applying iBLFs, the output/state constraints can be handled directly. However, feasibility conditions for virtual control signals are usually needed (Zhao and Song, 2019). Another effective way to handle output/state constraints is nonlinear mapping (NM). When using NM, the considered system can be transformed into a new system that is free of constraints. Then, the controller is designed based on the transformed system, so that the state constraints of the system will not be violated. To settle the output constraints, a log-type NM function was proposed by Guo and Wu (2014). A neural DSC approach for state-constrained systems using log-type NM was presented by Zhang et al. (2017). A command filter backstepping state-constrained control scheme for multi-input multi-output (MIMO) systems using NM was designed by Qiu et al. (2020), and Liu YL et al. (2018) extended this work to asymmetric time-varying constraints. Some new forms of NM have also been put forward to handle the problem of output/state constraints, such as tanh-type NM (Hua and Zhang, 2020a) and fraction-type NM. However, if there are no requirements for state constraints, the restrictions of state constraints cannot be ignored in these studies.

It is noticed that the above studies cannot guarantee that the system will achieve the control goal in finite time. Different from infinite-time control approaches, finite-time control approaches have better robustness and tracking performance. Recently, many studies have been done on finite-time control of nonlinear uncertain systems (Miao et al., 2016; Wang F et al., 2018; Li YM et al., 2019; Xue et al., 2020). Among them, Wang F et al. (2018) proposed an adaptive fuzzy finite-time control method. A finite-time adaptive DSC approach for MIMO uncertain systems was developed by Li YM et al. (2019), a fuzzy finite-time command filtered control scheme was developed by Yu et al. (2018), and Xia et al. (2019) performed studies of finite-time control for systems subject to state constraints. In previous studies, an exponential parameter $0 < \imath < 1$ was used in the virtual control laws. Unfortunately, when tracking errors converge to zero, the time derivative of the virtual control laws will grow infinitely. To avoid this problem, a C^1 smooth finite-time NN control scheme using a log-type BLF was proposed by Cui B et al. (2020).

The above-mentioned studies are based on time-triggered methods. To save communication resources, event-triggered control (ETC) approaches have received much attention. ETC-related methods have been studied using FLSs or NNs (Liu TF and Jiang, 2015; Sahoo et al., 2016; Wang YY et al., 2019; Zhu et al., 2020). Among them, ETC schemes were investigated with the help of input-to-state stability (ISS) (Liu TF and Jiang, 2015; Sahoo et al., 2016; Wang YC et al., 2017). To remove the ISS assumption, an ETC-based adaptive approach for uncertain nonlinear systems was proposed by Xing et al. (2017). ETC approaches have been applied widely in other systems (Li BW et al., 2018; Demirel et al., 2019; Liu Y et al., 2020; Xu et al., 2020; Zhu et al., 2020). Recently, finite-time control methods using event-triggered strategies were also investigated (Chen MH et al., 2020). An adaptive event-triggered finite-time control scheme was proposed by Chen MH et al. (2020), and event-triggered state-constrained control method was investigated by Wang YC et al. (2020). However, the event-triggered finite-time state-constrained control problem has not been mentioned.

Motivated by existing results, an event-triggered adaptive smooth finite-time DSC approach for MIMO uncertain nonlinear systems under asymmetric time-varying full state constraints is provided. The contributions of this paper are summarized as follows:

1. A novel NM function is introduced to transform an asymmetric time-varying state-constrained system into a new system that is free of constraints. Different from existing NM-based control methods (Guo and Wu, 2014; Hua and Zhang, 2020a; Zhao and Song, 2020), the tan-type NM-based control scheme is also available without state constraint requirements. Different from the tan-type NM-based method proposed by Wei et al. (2020a), we extend this work to deal with asymmetric time-varying constraints.

2. A new ETC-based smooth finite-time DSC approach is introduced for state-constrained systems. Note that some finite-time DSC-based control strategies have been developed (Li YM et al., 2019). However, when the tracking errors converge to zero,

the time derivative of the virtual control laws grows infinitely. To solve this problem, smooth switch functions are applied to the virtual laws. Then, the singularity in the traditional finite-time DSC can be avoided. Different from the smooth finite-time approach using BLFs by Cui B et al. (2020), a tan-type NM is applied to settle the state constraints directly. Moreover, an ETC rule is introduced to reduce the burden of communication while maintaining the stability of the state-constrained system.

2 Problem formulation and preliminaries

2.1 System description

Given a class of MIMO nonlinear systems in the following strict-feedback form:

$$\begin{cases} \dot{x}_{j,r_j} = F_{j,r_j}(\bar{\boldsymbol{x}}_{j,r_j}) + G_{j,r_j}(\bar{\boldsymbol{x}}_{j,r_j})x_{j,r_j+1}, \\ \quad j = 1, 2, \cdots, n,\ r_j = 1, 2, \cdots, m_j - 1, \\ \dot{x}_{j,m_j} = F_{j,m_j}(\boldsymbol{X}, \bar{\boldsymbol{\tau}}_{j-1}) + G_{j,m_j}(\bar{\boldsymbol{x}}_{j,m_j})\tau_j(t), \\ y_j = x_{j,1}, \end{cases} \tag{1}$$

where $\bar{\boldsymbol{x}}_{j,r_j} = \left[x_{j,1}, x_{j,2}, \cdots, x_{j,r_j}\right]^{\mathrm{T}} \in \mathbb{R}^{r_j}$, x_{j,r_j} and x_{j,m_j} denote the system states, $F_{j,r_j}(\bar{\boldsymbol{x}}_{j,r_j})$ and $F_{j,m_j}(\boldsymbol{X}, \bar{\boldsymbol{\tau}}_{j-1})$ are smooth nonlinear functions, $\boldsymbol{X} = \left[\boldsymbol{x}_1^{\mathrm{T}}, \boldsymbol{x}_2^{\mathrm{T}}, \cdots, \boldsymbol{x}_j^{\mathrm{T}}\right]^{\mathrm{T}}$ with $\boldsymbol{x}_j = \left[x_{j,1}, x_{j,2}, \cdots, x_{j,m_j}\right]^{\mathrm{T}}$, $G_{j,r_j}(\bar{\boldsymbol{x}}_{j,r_j})$ and $G_{j,m_j}(\bar{\boldsymbol{x}}_{j,m_j})$ are nonzero control gains, $\tau_j(t)$ is the control inputs with $\bar{\boldsymbol{\tau}}_{j-1} = \left[\tau_1, \tau_2, \cdots, \tau_{j-1}\right]^{\mathrm{T}} \in \mathbb{R}^{j-1}$, and $\boldsymbol{y} = [y_1, y_2, \cdots, y_n]^{\mathrm{T}} \in \mathbb{R}^n$ denotes the system output.

The aim of this work is to design an event-triggered adaptive finite-time fuzzy control approach using a tan-type NM, such that the asymmetric time-varying state constraints are never transgressed and y_j can follow the reference signal $y_{\mathrm{d}j}$ in finite time.

Remark 1 The system described in Eq. (1) is a general MIMO strict-feedback system that can be found in many practical applications, such as robotic systems (Zhang et al., 2018), aero vehicle systems (Hua and Zhang, 2020b), and underwater vehicle systems (Wang LJ et al., 2020). Meanwhile, output/state constraints often exist in these systems.

Assumption 1 The control gain G_{j,r_j} is bounded. The control gain G_{j,m_j} is known and bounded. There exist constants $g_0 > 0$ and $g_1 > 0$ such that $0 < g_0 < |G_{j,r_j}| < g_1$.

Assumption 2 The reference signal $y_{\mathrm{d}j}(t)$ satisfies $y_{\mathrm{d}j}(t) \in \varpi_y := \{|y_{\mathrm{d}j}(t)| < b_{\mathrm{d}j,1} < b_{j,1},\ \forall t > 0\}$, where $b_{\mathrm{d}j,1} > 0$ and $b_{j,1} > 0$ are constants. Meanwhile, the j^{th}-order derivatives of $y_{\mathrm{d}j}(t)$ ($j = 1, 2, ..., n$) are continuous and bounded.

2.2 Finite time

Definition 1 (Wang F et al., 2018) Consider the system $\varsigma = \phi(\varsigma, \tau)$, $\varsigma(t_0) = \varsigma_0$. If a constant ι and a settling time $T_{\mathrm{s}} < \infty$ exist, where $|\varsigma| \le \iota$, $\forall t \ge t_0 + T_{\mathrm{s}}$, then the equilibrium point $\varsigma = 0$ of the system is semi-globally practical finite-time stable (SGPFS).

Lemma 1 (Hardy et al., 1952) For $\forall \omega \in \mathbb{R}$ and $0 < \imath < 1$, the following inequality holds:

$$\left(\sum_{j=1}^{m} |\omega_j|\right)^{\imath} \le \sum_{j=1}^{m} |\omega_j|^{\imath} \le m^{1-\imath}\left(\sum_{j=1}^{m} |\omega_j|\right)^{\imath}. \tag{2}$$

Lemma 2 (Qian and Lin, 2001) For any variables χ_1 and χ_2 and positive constants ς_1, ς_2, and ς_3, one has

$$\begin{aligned} |\chi_1|^{\varsigma_1}|\chi_2|^{\varsigma_2} \le & \frac{\varsigma_1}{\varsigma_1 + \varsigma_2}\varsigma_3|\chi_1|^{\varsigma_1+\varsigma_2} \\ & + \frac{\varsigma_2}{\varsigma_1 + \varsigma_2}\varsigma_3^{\frac{-\varsigma_1}{\varsigma_2}}|\chi_2|^{\varsigma_1+\varsigma_2}. \end{aligned} \tag{3}$$

Lemma 3 (Polycarpou, 1996) Considering the constant $\hbar > 0$ and $\forall \varsigma \in \mathbb{R}$, the following inequality holds:

$$0 \le |\varsigma| - \varsigma \tanh\left(\frac{\varsigma}{\hbar}\right) \le 0.2785\hbar. \tag{4}$$

Lemma 4 (Chen CLP et al., 2014) For $\varsigma_1, \varsigma_2 \in \mathbb{R}$, the following Young's inequality holds:

$$\varsigma_1\varsigma_2 \le \frac{\lambda^p}{p}|\varsigma_1|^p + \frac{1}{q\lambda^q}|\varsigma_2|^q, \tag{5}$$

where $\lambda > 0$, $p > 1$, and $q > 1$ with $(p-1)(q-1) = 1$.

Lemma 5 (Wang F et al., 2018) Consider the system $\varsigma = \phi(\varsigma, \tau)$ and the Lyapunov function $V(\varsigma)$. If there exist $c_1 > 0$, $c_2 > 0$, and $0 < \imath < 1$, so that

$$\dot{V}(\varsigma) \le -c_1 V^{\imath}(\varsigma) + c_2, \tag{6}$$

then the system $\varsigma = \phi(\varsigma, \tau)$ is SGPFS.

2.3 Fuzzy logic systems

FLSs are designed to compensate for unknown functions. The inference rules can be described as

$\mathcal{R}^\jmath$: If ς_1 is $H_1^\jmath$, ς_2 is $H_2^\jmath$, $\cdots$, and ς_n is $H_n^\jmath$, then y is $K^\jmath$ ($\jmath=1,2,\cdots,N$), where ς_j represents the FLS input, y is the FLS output, and N represents the number of rules. $H_r^\jmath$ and $K^\jmath$ are fuzzy sets, associated with the fuzzy membership functions $\mu_{H_i^\jmath}(\varsigma_r)$ and $\mu_{K^\jmath}(y)$, respectively.

By the singleton fuzzifier and center average defuzzification, the FLS can be described as

$$y(\varsigma)=\frac{\sum_{\jmath=1}^{N}\left[\bar{y}_\jmath\prod_{r=1}^{n}\mu_{H_i^\jmath}(\varsigma_r)\right]}{\sum_{\jmath=1}^{N}\prod_{r=1}^{n}\mu_{H_i^\jmath}(\varsigma_r)}, \tag{7}$$

where $\bar{y}_\jmath=\max\limits_{y\in\mathbb{R}}\mu_{K^\jmath}(y)$.

The fuzzy basis function is defined as

$$S_\jmath=\frac{\prod_{r=1}^{n}\mu_{H_i^\jmath}(\varsigma_r)}{\sum_{\jmath=1}^{N}\prod_{r=1}^{n}\mu_{H_i^\jmath}(\varsigma_r)}. \tag{8}$$

Denote $\boldsymbol{\Theta}^{\mathrm{T}}=[\bar{y}_1,\bar{y}_2,\cdots,\bar{y}_N]=[\Theta_1,\Theta_2,\cdots,\Theta_N]$ and $\boldsymbol{S}(\varsigma)=[S_1(\varsigma),S_2(\varsigma),\cdots,S_N(\varsigma)]^{\mathrm{T}}$. Then, Eq. (7) can be described as

$$y(\varsigma)=\boldsymbol{\Theta}^{\mathrm{T}}\boldsymbol{S}(\varsigma). \tag{9}$$

Lemma 6 (Tong et al., 2012) Consider a continuous function $h(\varsigma)$ which is defined on a compact set Ω. Then, a fuzzy logic system exists such that

$$\sup_{x\in\Omega}|h(\varsigma)-\boldsymbol{\Theta}^{\mathrm{T}}\boldsymbol{S}(\varsigma)|\leq\delta, \tag{10}$$

where $\delta>0$ is a bounded constant.

Define the optimal approximation weight as $\boldsymbol{\Theta}^*=\min\limits_{\varsigma\in\boldsymbol{\Theta}}\left[\sup\limits_{x\in\Omega}|h(\varsigma)-\boldsymbol{\Theta}^{\mathrm{T}}\boldsymbol{S}(\varsigma)|\right]$. The function $f(x)$ can be expressed as $f(\varsigma)=(\boldsymbol{\Theta}^*)^{\mathrm{T}}\boldsymbol{S}(\varsigma)+\bar{\delta}$, where $\bar{\delta}$ is a bounded constant.

2.4 Nonlinear mapping

Definition 2 A tan-type NM function $\xi(x)$ is defined as follows:

$$\varpi=q(x)\frac{2\bar{b}}{\pi}\tan\left(\frac{\pi x}{2\bar{b}}\right)+(1-q(x))\frac{2\underline{b}}{\pi}\tan\left(\frac{\pi x}{2\underline{b}}\right), \tag{11}$$

where

$$q(x)=\begin{cases}1,\ x\geq 0,\\ 0,\ x<0.\end{cases} \tag{12}$$

For ease of notation, $q(x)$ is abbreviated as q, and $\bar{b}>0$ and $\underline{b}>0$ are time-varying state constraints of x. Then we can obtain the time derivative of Eq. (11) as

$$\dot{\varpi}=\mu+\nu\dot{x}, \tag{13}$$

where μ and ν are given as follows:

$$\begin{aligned}\mu=&q\left[\frac{2\dot{\bar{b}}}{\pi}\tan\left(\frac{\pi x}{2\bar{b}}\right)-\frac{x\dot{\bar{b}}}{\bar{b}}\sec^2\left(\frac{\pi x}{2\bar{b}}\right)\right]\\&+(1-q)\left[\frac{2\dot{\underline{b}}}{\pi}\tan\left(\frac{\pi x}{2\underline{b}}\right)-\frac{x\dot{\underline{b}}}{\underline{b}}\sec^2\left(\frac{\pi x}{2\underline{b}}\right)\right],\end{aligned} \tag{14}$$

$$\nu=q\sec^2\left(\frac{\pi x}{2\bar{b}}\right)+(1-q)\sec^2\left(\frac{\pi x}{2\underline{b}}\right). \tag{15}$$

Using Eq. (13), the considered system (1) can be transformed as

$$\begin{cases}\dot{\varpi}_{j,r_j}=f_{j,r_j}+\varpi_{j,r_j+1}\\ \qquad s=1,2,\cdots,n,\ r_j=1,2,\cdots,m_j-1,\\ \dot{\varpi}_{j,m_j}=f_{j,m_j}+g_{j,m_j}\tau_j(t),\\ y_j^*=\varpi_{j,1},\end{cases} \tag{16}$$

where

$$\begin{aligned}f_{j,r_j}=&\nu_{j,r_j}\left(F_{j,r_j}+G_{j,r_j}x_{j,r_j+1}\right)\\&+\mu_{j,r_j}-\varpi_{j,r_j+1},\end{aligned} \tag{17}$$

$$f_{j,m_j}=\nu_{j,m_j}F_{j,m_j}+\mu_{j,m_j}, \tag{18}$$

$$g_{j,m_j}=\nu_{j,m_j}G_{j,m_j}. \tag{19}$$

Meanwhile, $y_{\mathrm{d}j}$ can be transformed as

$$y_{\mathrm{d}j}^*=q\frac{2\bar{b}_{j,1}}{\pi}\tan\left(\frac{\pi y_{\mathrm{d}j}}{2\bar{b}_{j,1}}\right)+(1-q)\frac{2\underline{b}_{j,1}}{\pi}\tan\left(\frac{\pi y_{\mathrm{d}j}}{2\underline{b}_{j,1}}\right). \tag{20}$$

Lemma 7 Consider the sets $\Omega_x=\{x_{j,r_j}(t):-\underline{b}_{j,r_j}<x_{j,r_j}(t)<\bar{b}_{j,r_j}\}$ and $\Omega_\varpi=\{\varpi_{j,r_j}(t):\varpi_{j,r_j}(t)\in\mathbb{R}\}$. For any initial condition satisfying $x_{j,r_j}(0)\in\Omega_x$, if the signal $\varpi_{j,r_j}(t)$ is bounded, then $x_{j,r_j}(t)\in\Omega_x,\ \forall t\geq 0$.

Proof The proof is provided in Appendix A.

Lemma 8 Consider the sets $\Omega_x=\{x_{j,r_j}(t):-\underline{b}_{j,r_j}<x_{j,r_j}(t)<\bar{b}_{j,r_j}\}$ and $\Omega_\varpi=\{\varpi_{j,r_j}(t):\varpi_{j,r_j}(t)\in\mathbb{R}\}$, and parameters $l^*,l\in\mathbb{R}$. If the signal $\varpi_{j,r_j}(t)\to l^*$, then $x_{j,r_j}(t)\to l=\xi^{-1}(l^*)$.

Proof The proof is provided in Appendix B.

Remark 2 We compare the proposed tan-type NM with the existing log-type NM (Guo and Wu, 2014). For fair comparison, we discuss only the case of symmetric constraints. That is, the state x_{j,r_j} is required to remain in the set $\Omega_x=\{x_{j,r_j}|-b_{j,r_j}\leq x_{j,r_j}\leq b_{j,r_j}\}$, where $b_{j,r_j}>0$ is a constraint.

When no state constraints are required, that is, $b_{j,r_j}\to\infty$, then we have

$$\lim_{b_{j,r_j}\to\infty}\varpi_{j,r_j}=\frac{2b_{j,r_j}}{\pi}\tan\left(\frac{\pi x_{j,r_j}}{2b_{j,r_j}}\right)=x_{j,r_j}. \tag{21}$$

When $b_{j,r_j} \to \infty$, the log-type NM proposed by Guo and Wu (2014) can be rewritten as

$$\lim_{b_{j,r_j}\to\infty} \varpi_{j,r_j} = \lg\left(\frac{b_{j,r_j}+x_{j,r_j}}{b_{j,r_j}-x_{j,r_j}}\right) = 0. \tag{22}$$

It can be seen from Eq. (21) that when $b_{j,r_j} \to \infty$, $\varpi_{j,r_j} \to x_{j,r_j}$. Thus, the states of the original system will not be affected by the tan-type NM. However, from Eq. (22) we can see that when $b_{j,r_j} \to \infty$, $\varpi_{j,r_j} \to 0$. Therefore, tan-type NM is a versatile function, which is more suitable to handle state constraint problems.

Remark 3 It is noticed that a tan-type NM was proposed in our previous paper (Wei et al., 2020a). However, the tan-type NM proposed in Wei et al. (2020a) was a symmetrical one. In this study, we extend tan-type nonlinear mapping to solve the problem of asymmetric state constraints. That is to say, compared with the old tan-type NM, the new tan-type NM is a more general one.

3 Event-triggered finite-time controller design

Fig. 1 shows the main structure of the designed control method. First, the error equations are defined as

$$\chi_{j,1} = \varpi_{j,1} - y^*_{\mathrm{d}j}, \tag{23}$$

$$\chi_{j,r_j} = \varpi_{j,r_j} - v^{\mathrm{c}}_{j,r_j}, \tag{24}$$

$$z_{j,r_j} = v^{\mathrm{c}}_{j,r_j} - v_{j,r_j-1}, \tag{25}$$

where $\chi_{j,1}$ denotes the tracking error, χ_{j,r_j} denotes the error surface, v_{j,r_j} is the virtual control law, and v^{c}_{j,r_j} denotes the filtered value of v_{j,r_j}.

1. Step $j,1$ $(j = 1, 2, \cdots, n)$

According to Eqs. (16), (23), and (24), the time derivative of $\chi_{j,1}$ is given by

$$\dot{\chi}_{j,1} = f_{j,1} + \varpi_{j,2} + v_{j,1} + z_{j,2} - \dot{y}^*_{\mathrm{d}j}. \tag{26}$$

Construct the Lyapunov function candidate (LFC) as follows:

$$V_{j,1} = \frac{1}{2}\chi^2_{j,1} + \frac{1}{2\gamma_{j,1}}\tilde{\boldsymbol{\Theta}}^{\mathrm{T}}_{j,1}\tilde{\boldsymbol{\Theta}}_{j,1}, \tag{27}$$

where $\gamma_{j,1} > 0$ is a constant, $\tilde{\boldsymbol{\Theta}}_{j,1} = \boldsymbol{\Theta}^*_{j,1} - \hat{\boldsymbol{\Theta}}_{j,1}$, $\boldsymbol{\Theta}^*_{j,1}$ denotes the optimal weight, and $\hat{\boldsymbol{\Theta}}_{j,1}$ denotes the adaptive weight.

Differentiating $V_{j,1}$ respective to time and considering Eq. (26), we have

$$\begin{aligned}\dot{V}_{j,1} =& \chi_{j,1}\big(\boldsymbol{\Theta}^{*\mathrm{T}}_{j,1}\boldsymbol{S}_{j,1} + \bar{\boldsymbol{\Theta}}_{j,1} + \varpi_{j,2} + v_{j,1} + z_{j,2} \\ & - \dot{y}^*_{\mathrm{d}j}\big) - \frac{1}{\gamma_{j,1}}\tilde{\boldsymbol{\Theta}}^{\mathrm{T}}_{j,1}\dot{\hat{\boldsymbol{\Theta}}}_{j,1}.\end{aligned} \tag{28}$$

We design the virtual control law as follows:

$$v_{j,1} = -\frac{3}{2}\chi_{j,1} - k_{j,1}\alpha_{j,1}(\chi_{j,1}) - \hat{\boldsymbol{\Theta}}^{\mathrm{T}}_{j,1}\boldsymbol{S}_{j,1} + \dot{y}^*_{\mathrm{d}j}, \tag{29}$$

where $k_{j,1} > 0$ is a constant. $\alpha_{j,1}(\chi_{j,1})$ is a smooth switch function, which is defined as

$$\alpha_{j,1}(\chi_{j,1}) = \begin{cases} \chi^{2\imath-1}_{j,1}, & |\chi_{j,1}| \geq \epsilon_{j,1}, \\ \varrho_{j,1}\chi_{j,1} + h_{j,1}\chi^3_{j,1}, & |\chi_{j,1}| < \epsilon_{j,1}, \end{cases} \tag{30}$$

where $\epsilon_{j,1}$ is a small positive constant, $\varrho_{j,1} = (2-\imath)\epsilon^{2\imath-2}_{j,1}$, and $h_{j,1} = (\imath-1)\epsilon^{2\imath-4}_{j,1}$.

The adaptive law is presented as follows:

$$\dot{\hat{\boldsymbol{\Theta}}}_{j,1} = \gamma_{j,1}\left(\chi_{j,1}\boldsymbol{S}_{j,1} - \kappa_{j,1}\hat{\boldsymbol{\Theta}}_{j,1}\right), \tag{31}$$

where $\gamma_{j,1} > 0$ and $\kappa_{j,1} > 0$ are constants. Substi-

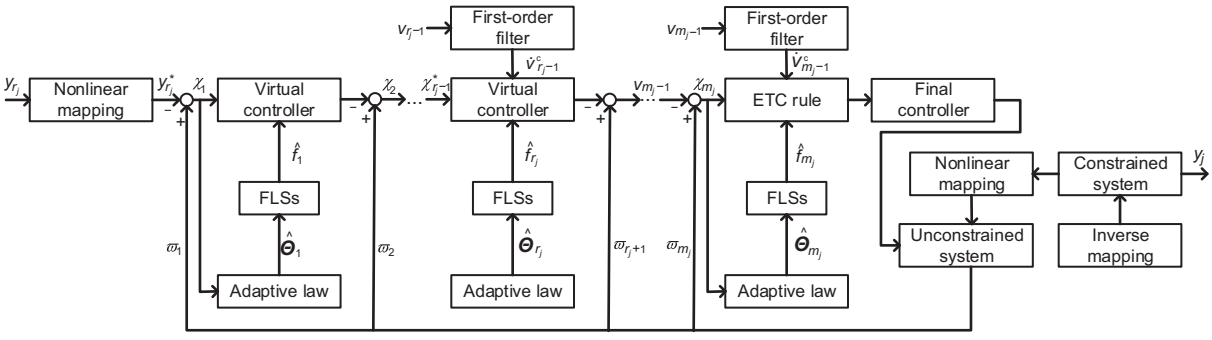

Fig. 1 Block diagram of the proposed control approach

tuting Eqs. (29) and (31) into Eq. (28), we have

$$\begin{aligned}\dot{V}_{j,1} =& -\frac{3}{2}\chi_{j,1}^2 - k_{j,1}\chi_{j,1}\alpha_{j,1}(\chi_{j,1}) + \kappa_{j,1}\tilde{\boldsymbol{\theta}}_{j,1}^{\mathrm{T}}\hat{\boldsymbol{\theta}}_{j,1}\\ &+ \chi_{j,1}\left(\bar{\delta}_{j,1} + \chi_{j,2} + z_{j,2}\right).\end{aligned} \tag{32}$$

Using Young's inequality, we have

$$\begin{cases}\chi_{j,1}(\bar{\delta}_{j,1} + \chi_{j,2} + z_{j,2})\\ \quad \le \dfrac{3}{2}\chi_{j,1}^2 + \dfrac{1}{2}\bar{\delta}_{j,1}^2 + \dfrac{1}{2}\chi_{j,2}^2 + \dfrac{1}{2}z_{j,2}^2,\\ \tilde{\boldsymbol{\theta}}_{j,1}^{\mathrm{T}}\hat{\boldsymbol{\theta}}_{j,1} \le \dfrac{1}{2}\left(\|\boldsymbol{\theta}_{j,1}^*\|^2 - \|\tilde{\boldsymbol{\theta}}_{j,1}^2\|\right).\end{cases} \tag{33}$$

Substituting inequality (33) into Eq. (32) yields

$$\begin{aligned}\dot{V}_{j,1} \le& -k_{j,1}\chi_{j,1}\alpha_{j,1}(\chi_{j,1}) - \frac{\kappa_{j,1}}{2}\|\tilde{\boldsymbol{\theta}}_{j,1}\|^2\\ &+ \frac{1}{2}\chi_{j,2}^2 + \frac{1}{2}z_{j,2}^2 + D_{j,1},\end{aligned} \tag{34}$$

where $D_{j,1} = \frac{\kappa_{j,1}}{2}\|\boldsymbol{\theta}_{j,1}^*\|^2 + \frac{1}{2}\bar{\delta}_{j,1}^2$.

2. Step j, r_j ($j = 1, 2, \cdots, n,\ r_j = 2, 3, \cdots, m-1$)

The time derivative of χ_{j,r_j} is given by

$$\begin{aligned}\dot{\chi}_{j,r_j} =& \boldsymbol{\theta}_{j,r_j}^{*\mathrm{T}}\boldsymbol{S}_{j,r_j} + \bar{\delta}_{j,r_j} + v_{j,r_j} + z_{j,r_j+1}\\ &+ \varpi_{j,r_j+1} - \dot{v}_{j,r_j}^{\mathrm{c}}.\end{aligned} \tag{35}$$

Consider the LFC as follows:

$$V_{j,r_j} = \frac{1}{2}\chi_{j,r_j}^2 + \frac{1}{2}z_{j,r_j}^2 + \frac{1}{2\gamma_{j,r_j}}\tilde{\boldsymbol{\theta}}_{j,r_j}^{\mathrm{T}}\tilde{\boldsymbol{\theta}}_{j,r_j}, \tag{36}$$

where $\gamma_{j,r_j} > 0$ is a design parameter, $\tilde{\boldsymbol{\theta}}_{j,r_j} = \boldsymbol{\theta}_{j,r_j}^* - \hat{\boldsymbol{\theta}}_{j,r_j}$, $\boldsymbol{\theta}_{j,r_j}^*$ denotes the optimal weight, and $\hat{\boldsymbol{\theta}}_{j,r_j}$ denotes the adaptive updating weight. Taking the time derivative of V_{j,r_j} yields

$$\dot{V}_{j,r_j} = \chi_{j,r_j}\dot{\chi}_{j,r_j} + z_{j,r_j}\dot{z}_{j,r_j} - \frac{1}{\gamma_{j,r_j}}\tilde{\boldsymbol{\theta}}_{j,r_j}^{\mathrm{T}}\dot{\hat{\boldsymbol{\theta}}}_{j,r_j}. \tag{37}$$

The first-order filter is introduced as follows:

$$\dot{v}_{j,r_j}^{\mathrm{c}} = -\sigma_{j,r_j}z_{j,r_j},\ v_{j,r_j}^{\mathrm{c}}(0) = v_{j,r_j-1}(0). \tag{38}$$

According to Eqs. (25) and (38), we have

$$\dot{z}_{j,r_j} = -\sigma_{j,r_j}z_{j,r_j} + \beta_{j,r_j}, \tag{39}$$

where β_{j,r_j} is a continuous function. Substituting Eqs. (35) and (39) into Eq. (37), we have

$$\begin{aligned}\dot{V}_{j,r_j} =& \chi_{j,r_j}\big(\boldsymbol{\theta}_{j,r_j}^{*\mathrm{T}}\boldsymbol{S}_{j,r_j} + \bar{\delta}_{j,r_j} + v_{j,r_j} + z_{j,r_j+1}\\ &+ \chi_{j,r_j+1} - \dot{v}_{j,r_j}^{\mathrm{c}}\big) - \frac{1}{\gamma_{j,r_j}}\tilde{\boldsymbol{\theta}}_{j,r_j}^{\mathrm{T}}\dot{\hat{\boldsymbol{\theta}}}_{j,r_j}\\ &+ z_{j,r_j}\left(-\sigma_{j,r_j}z_{j,r_j} + \beta_{j,r_j}\right).\end{aligned} \tag{40}$$

The virtual control law is designed as follows:

$$\begin{aligned}v_{j,r_j} =& -2\chi_{j,r_j} - k_{j,r_j}\alpha_{j,r_j}(\chi_{j,r_j})\\ &- \hat{\boldsymbol{\theta}}_{j,r_j}^{\mathrm{T}}\boldsymbol{S}_{j,r_j} + \dot{v}_{j,r_j}^{\mathrm{c}},\end{aligned} \tag{41}$$

where k_{j,r_j} is a positive constant. α_{j,r_j} is a smooth switch function provided as

$$\alpha_{j,r_j} = \begin{cases}\chi_{j,r_j}^{2\imath-1},\ |\chi_{j,r_j}| \ge \epsilon_{j,r_j},\\ \varrho_{j,r_j}\chi_{j,r_j} + h_{j,r_j}\chi_{j,r_j}^3,\ |\chi_{j,r_j}| < \epsilon_{j,r_j},\end{cases} \tag{42}$$

where ϵ_{j,r_j} is a small positive constant, $\varrho_{j,r_j} = (2-\imath)\epsilon_{j,r_j}^{2\imath-2}$, and $h_{j,r_j} = (\imath-1)\epsilon_{j,r_j}^{2\imath-4}$.

The adaptive law is designed as follows:

$$\dot{\hat{\boldsymbol{\theta}}}_{j,r_j} = \gamma_{j,r_j}\left(\chi_{j,r_j}\boldsymbol{S}_{j,r_j} - \kappa_{j,r_j}\hat{\boldsymbol{\theta}}_{j,r_j}\right), \tag{43}$$

where $\kappa_{j,r_j} > 0$ is a design constant. Substituting Eqs. (41) and (43) into Eq. (40) yields

$$\begin{aligned}\dot{V}_{j,r_j} =& -2\chi_{j,r_j}^2 - k_{j,r_j}\chi_{j,r_j}\alpha_{j,r_j}(\chi_{j,r_j})\\ &- \sigma_{j,r_j}z_{j,r_j}^2 + \chi_{j,r_j}\left(\bar{\delta}_{j,r_j} + z_{j,r_j+1} + \chi_{j,r_j+1}\right)\\ &+ z_{j,r_j}\beta_{j,r_j} + \kappa_{j,r_j}\tilde{\boldsymbol{\theta}}_{j,r_j}^{\mathrm{T}}\hat{\boldsymbol{\theta}}_{j,r_j}.\end{aligned} \tag{44}$$

Using Young's inequality, we have

$$\begin{cases}\chi_{j,r_j}\left(\bar{\delta}_{j,r_j} + z_{j,r_j+1} + \chi_{j,r_j+1}\right)\\ \quad \le \dfrac{3}{2}\chi_{j,r_j}^2 + \dfrac{1}{2}\bar{\delta}_{j,r_j}^2 + \dfrac{1}{2}z_{j,r_j+1}^2 + \dfrac{1}{2}\chi_{j,r_j+1}^2,\\ z_{j,r_j}\beta_{j,r_j} \le \dfrac{\beta_{j,r_j}^2}{2\vartheta^2}z_{j,r_j}^2 + \dfrac{1}{2}\vartheta^2,\\ \tilde{\boldsymbol{\theta}}_{j,r_j}^{\mathrm{T}}\hat{\boldsymbol{\theta}}_{j,r_j} \le \dfrac{1}{2}\left(\|\boldsymbol{\theta}_{j,r_j}^*\|^2 - \|\tilde{\boldsymbol{\theta}}_{j,r_j}\|^2\right),\end{cases} \tag{45}$$

where ϑ is a nonzero constant. Substituting inequality (45) into Eq. (44), we have

$$\begin{aligned}\dot{V}_{j,r_j} \le& -\frac{1}{2}\chi_{j,r_j}^2 - k_{j,r_j}\chi_{j,r_j}\alpha_{j,r_j}(\chi_{j,r_j}) + \frac{1}{2}\chi_{j,r_j+1}^2\\ &- \left(\sigma_{j,r_j} - \frac{\beta_{j,r_j}^2}{2\vartheta^2}\right)z_{j,r_j}^2 + \frac{1}{2}z_{j,r_j+1}^2\\ &- \frac{\kappa_{j,r_j}}{2}\|\tilde{\boldsymbol{\theta}}_{j,r_j}\|^2 + D_{j,r_j},\end{aligned} \tag{46}$$

where $D_{j,r_j} = \frac{1}{2}\vartheta^2 + \frac{1}{2}\bar{\delta}_{j,r_j}^2 + \frac{\kappa_{j,r_j}}{2}\|\boldsymbol{\theta}_{j,r_j}^*\|^2$.

3. Step j, m_j ($j = 1, 2, \cdots, n$)

Inspired by the studies in Xing et al. (2019), a relative threshold ETC is introduced in this step:

$$\tau_j(t) = w_j(t_k),\ \forall t \in [t_k, t_{k+1}), \tag{47}$$

$$t_{k+1}=\inf\{t>t_k||w_j(t)-\tau_j(t)|\geq d|w_j(t)|+\eta\}, \tag{48}$$

where $\tau_j(t)$ denotes the actual controller, $\inf\{\cdot\}$ denotes the infimum of $\{\cdot\}$, $w_j(t)$ is the control law, t_k denotes the updating time, and $0<d<1$ and $0<\eta<1$ are constants. When $t\in[t_k,t_{k+1})$, the actual control input $\tau_j(t)$ stays constant at $w_j(t_k)$. Then, we have

$$|w_j(t)-\tau_j(t)|\leq d|\tau_j(t)|+\eta,\ \forall t\geq 0. \tag{49}$$

Therefore, there exist $|s_1(t)|\leq 1$ and $|s_2(t)|\leq 1$, which makes the following equality holds:

$$w_j(t)=[1+s_1(t)d]\tau_j(t)+s_2(t)\eta. \tag{50}$$

Then we have

$$\tau_j(t)=\frac{w_j(t)}{1+s_1(t)d}-\frac{s_2(t)\eta}{1+s_1(t)d}. \tag{51}$$

The time derivative of χ_{j,m_j} is given as

$$\begin{aligned}\dot{\chi}_{j,m_j}=&(\boldsymbol{\theta}^*_{j,m_j})^{\mathrm{T}}\boldsymbol{S}_{j,m_j}+\bar{\delta}_{j,m_j}+g_{j,m_j}\tau_j(t)\\&-\dot{v}^{\mathrm{c}}_{j,m_j-1}.\end{aligned} \tag{52}$$

Consider the LFC as follows:

$$V_{j,m_j}=\frac{1}{2}\chi^2_{j,m_j}+\frac{1}{2}z^2_{j,m_j}+\frac{1}{2\gamma_{j,m_j}}\tilde{\boldsymbol{\theta}}^{\mathrm{T}}_{j,m_j}\tilde{\boldsymbol{\theta}}_{j,m_j}, \tag{53}$$

where γ_{j,m_j} is a positive constant, $\tilde{\boldsymbol{\theta}}_{j,m_j}=\boldsymbol{\theta}^*_{j,m_j}-\hat{\boldsymbol{\theta}}_{j,m_j}$, $\boldsymbol{\theta}^*_{j,m_j}$ denotes the optimal weight, and $\hat{\boldsymbol{\theta}}_{j,m_j}$ denotes the adaptive weight. Then, the time derivative of V_{j,m_j} is given as

$$\begin{aligned}\dot{V}_{j,m_j}=&\chi_{j,m_j}\dot{\chi}_{j,m_j}+z_{j,m_j}\dot{z}_{j,m_j}\\&-\frac{1}{\gamma_{j,m_j}}\tilde{\boldsymbol{\theta}}^{\mathrm{T}}_{j,m_j}\dot{\hat{\boldsymbol{\theta}}}_{j,m_j}.\end{aligned} \tag{54}$$

Similarly, the first-order filter is introduced as follows:

$$\dot{v}^{\mathrm{c}}_{j,m_j}=-\sigma_{j,m_j}z_{j,m_j},\ v^{\mathrm{c}}_{j,m_j}(0)=v_{j,m_j-1}(0). \tag{55}$$

According to Eqs. (25) and (38), we have

$$\dot{z}_{j,m_j}=-\sigma_{j,m_j}z_{j,m_j}+\beta_{j,m_j}. \tag{56}$$

Substituting Eqs. (52) and (56) into Eq. (54), we have

$$\begin{aligned}\dot{V}_{j,m_j}=&-\frac{3}{2}\chi^2_{j,m_j}-\chi_{j,m_j}\alpha_{j,m_j}+\chi_{j,m_j}\left[\frac{g_{j,m_j}w_j(t)}{1+s_1(t)d}\right.\\&\left.-\frac{g_{j,m_j}s_2(t)\eta}{1+s_1(t)d}+v_{j,m_j}+\bar{\delta}_{j,m_j}\right]\\&-\sigma_{j,m_j}z^2_{j,m_j}+z_{j,m_j}\beta_{j,m_j}\\&+\tilde{\boldsymbol{\theta}}^{\mathrm{T}}_{j,m_j}\left(\chi_{j,m_j}\boldsymbol{S}_{j,m_j}-\frac{1}{\gamma_{j,m_j}}\dot{\hat{\boldsymbol{\theta}}}_{j,m_j}\right),\end{aligned} \tag{57}$$

where v_{j,m_j} is given as follows:

$$\begin{aligned}v_{j,m_j}=&\frac{3}{2}\chi_{j,m_j}+k_{j,m_j}\alpha_{j,m_j}(\chi_{j,m_j})\\&+\hat{\boldsymbol{\theta}}^{\mathrm{T}}_{j,m_j}\boldsymbol{S}_{j,m_j}-\dot{v}^{\mathrm{c}}_{j,m_j-1},\end{aligned} \tag{58}$$

where k_{j,m_j} is a positive constant. α_{j,m_j} is a smooth switch function designed as

$$\alpha_{j,m_j}=\begin{cases}\chi^{2\imath-1}_{j,m_j},\ |\chi_{j,m_j}|\geq\epsilon_{j,m_j},\\ \varrho_{j,m_j}\chi_{j,m_j}+h_{j,m_j}\chi^3_{j,m_j},\ |\chi_{j,m_j}|<\epsilon_{j,m_j},\end{cases} \tag{59}$$

where ϵ_{j,m_j} is a small positive constant, $\varrho_{j,m_j}=(2-\imath)\epsilon^{2\imath-2}_{j,m_j}$, and $h_{j,m_j}=(\imath-1)\epsilon^{2\imath-4}_{j,m_j}$.

Using Young's inequality, we have

$$\begin{cases}\chi_{j,m_j}\bar{\delta}_{j,m_j}\leq\dfrac{1}{2}\chi^2_{j,m_j}+\dfrac{1}{2}\bar{\delta}^2_{j,m_j},\\ z_{j,m_j}\beta_{j,m_j}\leq\dfrac{\beta^2_{j,m_j}}{2\vartheta^2}z^2_{j,m_j}+\dfrac{1}{2}\vartheta^2.\end{cases} \tag{60}$$

Substituting inequality (60) into Eq. (57), we have

$$\begin{aligned}\dot{V}_{j,m_j}\leq&-\chi^2_{j,m_j}-\chi_{j,m_j}\alpha_{j,m_j}+\chi_{j,m_j}\left[\frac{g_{j,m_j}w_j(t)}{1+s_1(t)d}\right.\\&\left.-\frac{g_{j,m_j}s_2(t)\eta}{1+s_1(t)d}+v_{j,m_j}\right]+\frac{1}{2}\vartheta^2+\frac{1}{2}\bar{\delta}^2_{s,m_j}\\&+\tilde{\boldsymbol{\theta}}^{\mathrm{T}}_{j,m_j}\left(\chi_{j,m_j}\boldsymbol{S}_{j,m_j}-\frac{1}{\gamma_{j,m_j}}\dot{\hat{\boldsymbol{\theta}}}_{j,m_j}\right)\\&-\left(\sigma_{j,m_j}-\frac{\beta^2_{j,m_j}}{2\vartheta^2}\right)z^2_{j,m_j}.\end{aligned} \tag{61}$$

Then, the ETC approach and the adaptive law are designed as follows:

$$\begin{aligned}w_j(t)=&-g^{-1}_{j,m_j}(1+d)v_{j,m_j}\tanh\left(\frac{\chi_{j,m_j}v_{j,m_j}}{\hbar}\right)\\&-g^{-1}_{j,m_j}\eta(1+d)\tanh\left(\frac{\chi_{j,m_j}\eta}{\hbar}\right),\end{aligned} \tag{62}$$

$$\dot{\hat{\boldsymbol{\theta}}}_{j,m_j}=\gamma_{j,m_j}\left(\chi_{j,m_j}\boldsymbol{S}_{j,m_j}-\kappa_{j,m_j}\hat{\boldsymbol{\theta}}_{j,m_j}\right), \tag{63}$$

where $\hbar>0$ and $\kappa_{j,m_j}>0$ are constants. Substituting Eqs. (62) and (63) into inequality (61) yields

$$\begin{aligned}\dot{V}_{j,m_j}\leq&-\chi_{j,m_j}^2-\chi_{j,m_j}\alpha_{j,m_j}+\chi_{j,m_j}\upsilon_{j,m_j}\\&-\frac{1+d}{1+s_1(t)d}\chi_{j,m_j}\upsilon_{j,m_j}\tanh\left(\frac{\chi_{j,m_j}\upsilon_{j,m_j}}{\hbar}\right)\\&-\frac{1+d}{1+s_1(t)d}\chi_{j,m_j}\eta\tanh\left(\frac{\chi_{j,m_j}\eta}{\hbar}\right)\\&-\frac{g_{j,m_j}s_2(t)}{1+s_1(t)d}\chi_{j,m_j}\eta+\kappa_{j,m_j}\tilde{\boldsymbol{\theta}}_{j,m_j}^{\mathrm{T}}\hat{\boldsymbol{\theta}}_{j,m_j}\\&-\left(\sigma_{j,m_j}-\frac{\beta_{j,m_j}^2}{2\vartheta^2}\right)z_{j,m_j}^2+\frac{1}{2}\vartheta^2+\frac{1}{2}\bar{\delta}_{s,m_j}^2.\end{aligned}\tag{64}$$

Using Young's inequality, Lemma 3, and the fact $1+s_1(t)d<1+d$, we have

$$\begin{cases}-\dfrac{1+d}{1+s_1(t)d}\chi_{j,m_j}\upsilon_{j,m_j}\tanh\left(\dfrac{\chi_{j,m_j}\upsilon_{j,m_j}}{\hbar}\right)\\\quad\leq-|\chi_{j,m_j}\upsilon_{j,m_j}|+0.2785\hbar,\\-\dfrac{1+d}{1+s_1(t)d}\chi_{j,m_j}\eta\tanh\left(\dfrac{\chi_{j,m_j}\eta}{\hbar}\right)\\\quad\leq-|\chi_{j,m_j}\eta|+0.2785\hbar,\\\tilde{\boldsymbol{\theta}}_{j,m_j}^{\mathrm{T}}\hat{\boldsymbol{\theta}}_{j,m_j}\leq\dfrac{1}{2}\left(\|\boldsymbol{\theta}_{j,m_j}^*\|^2-\|\tilde{\boldsymbol{\theta}}_{j,m_j}\|^2\right).\end{cases}\tag{65}$$

From Assumption 1, we have that G_{j,m_j} is known and bounded. Then, g_{j,m_j} is also bounded. Therefore, there exist positive constants $\bar{g}_{j,m_j}$ and $\underline{g}_{j,m_j}$, such that $0<\underline{g}_{j,m_j}<|g_{j,m_j}|<\bar{g}_{j,m_j}$. Thus, the following inequality holds:

$$-\frac{g_{j,m_j}s_2(t)}{1+s_1(t)d}\chi_{j,m_j}\eta\leq\frac{1}{2}\chi_{j,m_j}^2+\frac{1}{2}\bar{g}_{j,m_j}^2\eta^2.\tag{66}$$

Substituting inequality (65) into inequality (66) yields

$$\begin{aligned}\dot{V}_{j,m_j}\leq&-\frac{1}{2}\chi_{j,m_j}^2-\chi_{j,m_j}\alpha_{j,m_j}-\frac{\kappa_{j,m_j}}{2}\|\tilde{\boldsymbol{\theta}}_{j,m_j}\|^2\\&-\left(\sigma_{j,m_j}-\frac{\beta_{j,m_j}^2}{2\vartheta^2}\right)z_{j,m_j}^2+D_{j,m_j},\end{aligned}\tag{67}$$

where $D_{j,m_j}=0.557\hbar+\frac{1}{2}\bar{g}_{j,m_j}^2\eta^2+\frac{1}{2}\vartheta^2+\frac{1}{2}\bar{\delta}_{s,m_j}^2+\frac{1}{2}\|\boldsymbol{\theta}_{j,m_j}^*\|^2$.

Remark 4 For most kinds of state-constrained control methods based on log-type BLFs (Liu YJ et al., 2020), integral BLFs (Tee and Ge, 2011), and tan-type BLFs (Jin, 2016), feasibility conditions on virtual controllers are all required. It can be seen from Section 3 that the designed control approach in this study can handle the state constraints directly without any feasibility conditions.

Remark 5 We can see from Eqs. (30), (42), and (59) that $\alpha_{j,r_j}(\epsilon_{j,r_j}^+)=\alpha_{j,r_j}(\epsilon_{j,r_j}^-)=\epsilon_{j,r_j}^{2\imath-1}$ and $\dot{\alpha}_{j,r_j}(\epsilon_{j,r_j}^+)=\dot{\alpha}_{j,r_j}(\epsilon_{j,r_j}^-)=2\imath-1\epsilon_{j,r_j}^{2\imath-2}$. Thus, $\alpha_{j,r_j}(\chi_{j,r_j})$ are smooth switch functions. When $|\chi_{j,r_j}|\in[0,\ \epsilon_{j,r_j}]$, the time derivative of the virtual control signals remains bounded. Different from the C^1 smooth finite-time control approach proposed by Cui B et al. (2020), the proposed control method is an ETC approach. Using the event-triggered rule, communication resources can be saved.

4 Stability analysis

Theorem 1 Consider system (1), with Assumptions 1 and 2, under the virtual control laws (29), (41), and (58), the adaptive laws (31), (43), and (63), and the final control law (62), with the initial states satisfying $x_{j,r_j}(0)\in\Omega_x=\{x_{j,r_j}(t):-\underline{b}_{j,r_j}<x_{j,r_j}(t)<\bar{b}_{j,r_j}\}$. Then, we have the following conclusions: (1) The closed-loop system is SGPFS; (2) All signals of the closed-loop system are bounded, and $x_{j,r_j}(t)\in\Omega_x,\ \forall t\geq0$; (3) There exists a time constant t_{r} satisfying $t_{k+1}-t_k\geq t_{\mathrm{r}}$.

Proof The LFC is constructed as follows:

$$V=\sum_{j=1}^{n}\sum_{r_j=1}^{m}V_{j,r_j}.\tag{68}$$

Differentiating V and considering inequalities (34), (46), and (67), we have

$$\begin{aligned}\dot{V}\leq&\sum_{j=1}^{n}\sum_{r_j=1}^{m}\Bigg(-k_{j,r_j}\chi_{j,r_j}\alpha_{j,r_j}-\frac{\kappa_{j,r_j}}{2}\|\tilde{\boldsymbol{\theta}}_{j,r_j}\|^2\\&+D_{j,r_j}\Bigg)-\sum_{j=1}^{n}\sum_{r_j=2}^{m}\bar{\sigma}_{j,r_j}z_{j,r_j}^2,\end{aligned}\tag{69}$$

where $\bar{\sigma}_{j,r_j}=\sigma_{j,r_j}-\frac{\beta_{j,r_j}^2}{2\vartheta^2}$. The proof is divided into two cases:

Case 1: When $|\chi_{j,r_j}|\geq\epsilon_{j,r_j}$, substituting $\alpha_{j,r_j}=\chi_{j,r_j}^{2\imath-1}$ into inequality (69) yields

$$\begin{aligned}\dot{V}\leq&\sum_{j=1}^{n}\sum_{r_j=1}^{m}\Bigg(-k_{j,r_j}\chi_{j,r_j}^{2\imath}-\frac{\kappa_{j,r_j}}{2}\|\tilde{\boldsymbol{\theta}}_{j,r_j}\|^2\\&+D_{j,r_j}\Bigg)-\sum_{j=1}^{n}\sum_{r_j=2}^{m}\bar{\sigma}_{j,r_j}z_{j,r_j}^2.\end{aligned}\tag{70}$$

According to Lemma 2, let $\omega_1=1$, $\omega_2=\|\tilde{\boldsymbol{\Theta}}_{j,r_j}\|^2$, $\varsigma_1=\imath$, $\varsigma_2=1-\imath$, and $\varsigma_3=\imath^{\frac{1-\imath}{\imath}}$. So we have

$$\|\tilde{\boldsymbol{\Theta}}_{j,r_j}\|^{2\imath}\leq\imath\varsigma_3+\|\tilde{\boldsymbol{\Theta}}_{j,r_j}\|^2. \tag{71}$$

Similarly, let $\omega_1=1$, $\omega_2=z_{j,r_j}^2$, $\varsigma_1=\imath$, $\varsigma_2=1-\imath$, and $\varsigma_3=\imath^{\frac{1-\imath}{\imath}}$. We have

$$z_{j,r_j}^{2\imath}\leq\imath\varsigma_3+z_{j,r_j}^2. \tag{72}$$

Substituting inequalities (71) and (72) into inequality (70), we have

$$\begin{aligned}\dot{V}\leq&\sum_{j=1}^{n}\sum_{r_j=1}^{m}\left(-k_{j,r_j}\chi_{j,r_j}^{2\imath}-\frac{\kappa_{j,r_j}}{2}\|\tilde{\boldsymbol{\Theta}}_{j,r_j}\|^{2\imath}\right)\\&-\sum_{j=1}^{n}\sum_{r_j=2}^{m}\bar{\sigma}_{j,r_j}z_{j,r_j}^{2\imath}+C_2,\end{aligned} \tag{73}$$

where $C_2=\sum_{j=1}^{n}\sum_{r_j=1}^{m}\left(\imath\varsigma_3+D_{j,r_j}\right)+\sum_{j=1}^{n}\sum_{r_j=2}^{m}\imath\varsigma_3$. Using Lemma 1, inequality (73) can be expressed as

$$\dot{V}\leq-C_1V^{\imath}+C_2, \tag{74}$$

where $C_1=\min\{2^{\imath}k_{j,r_j},\ 2^{\imath-1}\kappa_{j,r_j}\gamma_{j,r_j},\ 2^{\imath}\bar{\sigma}_{j,r_j}\}$.

Case 2: When $|\chi_{j,r_j}|<\epsilon_{j,r_j}$, substituting $\alpha_{j,r_j}=\varrho_{j,r_j}\chi_{j,r_j}+h_{j,r_j}\chi_{j,r_j}^3$ into inequality (69) yields

$$\begin{aligned}\dot{V}\leq&\sum_{j=1}^{n}\sum_{r_j=1}^{m}\Bigg(-k_{j,r_j}\varrho_{j,r_j}\chi_{j,r_j}^2-\frac{\kappa_{j,r_j}}{2}\|\tilde{\boldsymbol{\Theta}}_{j,r_j}\|^2\\&+k_{j,r_j}|h_{j,r_j}|\epsilon_{j,r_j}^4+D_{j,r_j}\Bigg)-\sum_{j=1}^{n}\sum_{r_j=2}^{m}\bar{\sigma}_{j,r_j}z_{j,r_j}^2.\end{aligned} \tag{75}$$

Using Lemma 1, inequality (74) can be changed to

$$\dot{V}\leq-C_3V+C_4, \tag{76}$$

where $C_3=\min\{2^{\imath}k_{j,r_j}\varrho_{j,r_j},\ 2^{\imath-1}\kappa_{j,r_j}\gamma_{j,r_j},\ 2^{\imath}\bar{\sigma}_{j,r_j}\}$ and $C_4=\sum_{j=1}^{n}\sum_{r_j=1}^{m}\left(k_{j,r_j}|h_{j,r_j}|\epsilon_{j,r_j}^4+D_{j,r_j}\right)$.

First, we will prove conclusion (1). When $|\chi_{j,r_j}|\geq\epsilon_{j,r_j}$, considering Lemma 5 and inequality (74), we can conclude that the closed-loop system is SGPFS. That is, a constant ι and a settling time $T_{\mathrm{s}}<\infty$ exist such that $|\chi_{j,r_j}|\leq\iota$, $\forall t\geq t_0+T_{\mathrm{s}}$. When $|\chi_{j,r_j}|<\epsilon_{j,r_j}$, we also have $|\chi_{j,r_j}|<\iota$. Therefore, we conclude that the whole system is SGPFS.

In the following, we will prove conclusion (2). From inequality (74) and the study by Wang F et al. (2018), we have $V\leq\left(\frac{C_2}{(1-\ell)C_1}\right)^{\imath}$, for $t\geq t_0+T_{\mathrm{s}}$. From inequality (76), we have $V\leq V(0)\mathrm{e}^{-C_3}+\frac{C_4}{C_3}$. Thus, V is bounded. Considering Eq. (68), it follows that χ_{j,r_j}, z_{j,r_j}, and $\tilde{\boldsymbol{\Theta}}_{j,r_j}$ are bounded. Thus, we have that ϖ_{j,r_j}, $\hat{\boldsymbol{\Theta}}_{j,r_j}$, and $\upsilon_{j,r_j}^{\mathrm{c}}$ are all bounded. Because ϖ_{j,r_j} is bounded, from Lemma 7, we can determine that the state constraints are not transgressed.

Finally, we will prove that conclusion (3) can be achieved. Define the control sampling error as $\varepsilon(t)=w(t)-\tau(t)$, $\forall t\in[t_k,\ t_{k+1})$. Then, we can obtain

$$\frac{\mathrm{d}}{\mathrm{d}t}|\varepsilon(t)|=\frac{\mathrm{d}}{\mathrm{d}t}(\varepsilon^2)^{\frac{1}{2}}=\mathrm{sign}(\varepsilon)\dot{\varepsilon}\leq|\dot{w}(t)|. \tag{77}$$

From Eq. (62), it can be seen that $\dot{w}_j(t)$ is a continuous and bounded function. Therefore, there exists a constant Q such that $|\dot{w}(t)|\leq Q$. From Eq. (62), we have $\varepsilon(t_k)=0$ and $\lim_{t\to t_{k+1}}\varepsilon(t)=d|w_j(t)|+\eta>\eta$. Then, the lower bound of the inter-execution interval t_{r} satisfies $t_{\mathrm{r}}\geq\frac{\eta}{Q}$. Thus, Zeno behavior is avoided.

Remark 6 From inequalities (74) and (76), we can obtain some suggestions on parameter selection. To achieve a smaller tracking error, we can enlarge C_1 and C_3 while reducing C_2 and C_4. Hence, we can select large k_{j,r_j} and $\kappa_{j,r_j}\gamma_{j,r_j}$, and small $\hbar$, η, and ϑ. Furthermore, the energy cost and the actual ability of the control force must be considered when selecting control parameters.

5 Simulation studies

In this section, two simulation examples are offered to validate the effectiveness of the designed ETC approach.

5.1 Example 1

Simulations of a fully actuated autonomous underwater vehicle (AUV) are offered. The motion functions of the AUV are described as follows:

$$\begin{cases}\dot{\boldsymbol{x}}_1=J(\psi)\boldsymbol{x}_2,\\\dot{\boldsymbol{x}}_2=\boldsymbol{F}(\boldsymbol{x}_2)+\boldsymbol{M}^{-1}\boldsymbol{\tau}(t),\\\boldsymbol{y}=\boldsymbol{x}_1,\end{cases} \tag{78}$$

where $\boldsymbol{x}_1=[x,\ y,\ \psi]^{\mathrm{T}}$ denotes the position and yaw angle of the AUV in the Earth frame, $\boldsymbol{x}_2=[u,\ v,\ r]^{\mathrm{T}}$ denotes the linear velocities and yaw angular velocity in the body frame, $J(\psi)$ is the rotation from the AUV body frame to the Earth frame, $\boldsymbol{M}$ is the inertia matrix, and $\boldsymbol{F}(\boldsymbol{x}_2)=\boldsymbol{M}^{-1}\left(C(\boldsymbol{x}_2)+D(\boldsymbol{x}_2)\right)\boldsymbol{x}_2$ denotes the nonlinear function. The detailed descriptions and the values of parameters can be found in Cui RX et al. (2017).

Using the NM function, Eq. (78) can be transformed as

$$\begin{cases} \dot{\boldsymbol{\varpi}}_1 = \boldsymbol{f}_1 + \boldsymbol{\varpi}_2, \\ \dot{\boldsymbol{\varpi}}_2 = \boldsymbol{f}_2 + \boldsymbol{g}_2\boldsymbol{\tau}(t), \\ \boldsymbol{y}^* = \boldsymbol{\varpi}_1, \end{cases} \tag{79}$$

where

$$\begin{cases} \boldsymbol{f}_1 = \boldsymbol{\nu}_1 (\boldsymbol{F}_1 + \boldsymbol{J}\boldsymbol{x}_2) + \boldsymbol{\mu}_1 - \boldsymbol{\varpi}_2, \\ \boldsymbol{f}_2 = \boldsymbol{\nu}_2 \boldsymbol{F}_2 + \boldsymbol{\mu}_2, \\ \boldsymbol{g}_2 = \boldsymbol{\nu}_2 \boldsymbol{J}. \end{cases} \tag{80}$$

Here, $\boldsymbol{\nu}_1$, $\boldsymbol{\nu}_2$, $\boldsymbol{\mu}_1$, and $\boldsymbol{\mu}_2$ can be obtained from Eqs. (14) and (15).

In this simulation, the function $\boldsymbol{f}_2 = [f_{1,2},\ f_{2,2},\ f_{3,2}]^{\mathrm{T}}$ is assumed to be unknown. An FLS is designed to compensate for the unknown function. The fuzzy membership functions are selected as

$$\mu_{H_{j,2}^{j}} = \exp_{j=1,2,\cdots,7}\left[-\frac{(x_{j,2}+4-j)^2}{4}\right],\ j = 1, 2, 3.$$

The control parameters are designed as $k_1 = k_2 = 5$, $\sigma_1 = 0.1$, $\imath = \frac{5}{7}$, $\epsilon_1 = \epsilon_2 = 0.1$, $d = 0.1$, $\eta = 0.3$, and $\hbar = 5$. The parameters of the adaptive weights are given as $\gamma_2 = 1$ and $\kappa_2 = 10$. The selected simulation time is $t = 20$ s. The initial states are $\boldsymbol{x}_1 = \left[-1,\ -1,\ \frac{\pi}{6}\right]^{\mathrm{T}}$ and $\boldsymbol{x}_2 = [0,\ 0,\ 0]^{\mathrm{T}}$. Other initial values are given as zero. The reference trajectories are selected as $x_{\mathrm{d}} = 1 + 2\sin\left(\frac{\pi t}{6}\right)$ and $y_{\mathrm{d}} = 1 - 2\cos\left(\frac{\pi t}{6}\right)$. Then, the desired yaw angle can be calculated as $\psi_{\mathrm{d}} = \arctan[2(\dot{y}_{\mathrm{d}}, \dot{x}_{\mathrm{d}})]$. The state constraints are selected as $\bar{\boldsymbol{b}}_1 = [5 + \sin\left(\frac{\pi t}{8}\right), 5 + \sin\left(\frac{\pi t}{8}\right), 5000]^{\mathrm{T}}$, $\underline{\boldsymbol{b}}_1 = [4+\sin t, 4+\sin t, 5000]^{\mathrm{T}}$, $\bar{\boldsymbol{b}}_2 = [5 + \sin t, 5 + \sin t, 5 + \sin t]^{\mathrm{T}}$, and $\underline{\boldsymbol{b}}_2 = [4, 4, 4]^{\mathrm{T}}$.

The simulation results are plotted in Figs. 2–6. The output-tracking performance under asymmetric time-varying state constraints is plotted in Fig. 2. At 4 and 12 s, the desired yaw angle ψ_{d} changes from $\frac{\pi}{2}$ to $-\frac{\pi}{2}$. Fig. 3 depicts the linear velocities and yaw angular velocity under constraints. The responses of the adaptive weights are plotted in Fig. 4. The ETC control law is shown in Fig. 5. The time intervals are plotted in Fig. 6. As we can see from Fig. 2, the system outputs can follow the reference trajectories well. From Fig. 2, the system can also achieve good trajectory tracking with large finite constraints. As observed in Figs. 2 and 3, no state constraints are violated. We can see from Figs. 2–5 that all signals are bounded. In Fig. 6, for $\tau_1(t)$, $\tau_2(t)$, and $\tau_2(t)$, the total numbers of triggers are 606, 450, and 278 respectively, and the numbers of non-triggering events

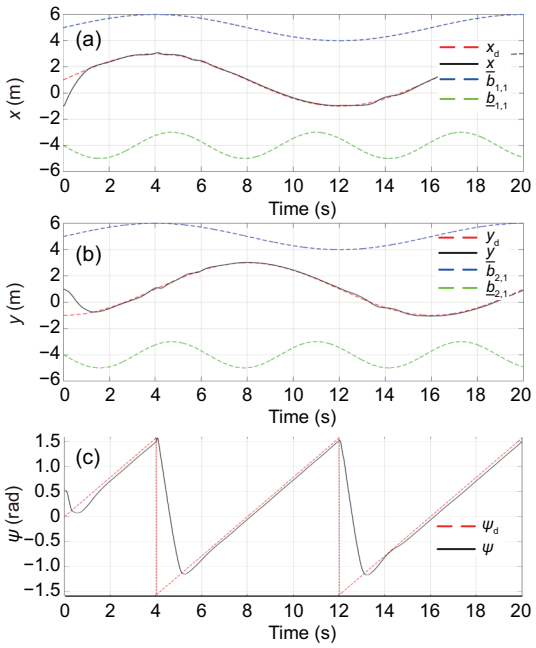

Fig. 2 Output-tracking performance under constraints x (a), y (b), and ψ (c) in Example 1

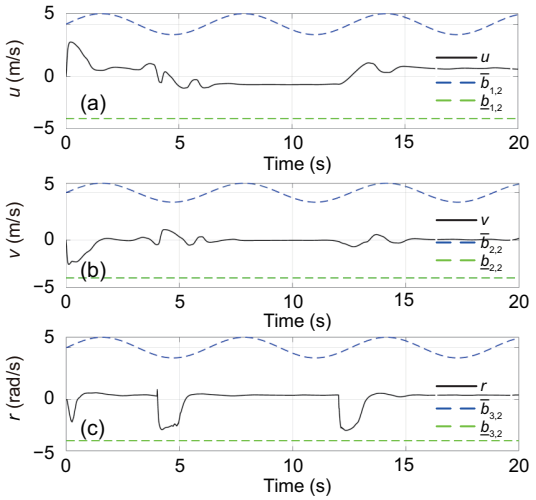

Fig. 3 Trajectories of the system states under constraints u (a), v (b), and r (c) in Example 1

are 1394, 1450, and 1722 respectively. Thus, using the designed ETC rule, the communication burden can be reduced significantly.

5.2 Example 2

Consider a two-degrees-of-freedom robot manipulator system with state constraint (Jin, 2016),

whose dynamics is presented as follows:

$$\begin{cases} \dot{\boldsymbol{x}}_1 = \boldsymbol{x}_2, \\ \boldsymbol{D}(\boldsymbol{x}_1)\dot{\boldsymbol{x}}_2 = \boldsymbol{\tau}(t) - \boldsymbol{C}(\boldsymbol{x}_1, \boldsymbol{x}_2)\boldsymbol{x}_2 - \boldsymbol{G}(\boldsymbol{x}_1) \\ \qquad\qquad - \boldsymbol{F}(\boldsymbol{x}_1, \boldsymbol{x}_2, t), \\ \boldsymbol{y} = \boldsymbol{x}_1, \end{cases} \tag{81}$$

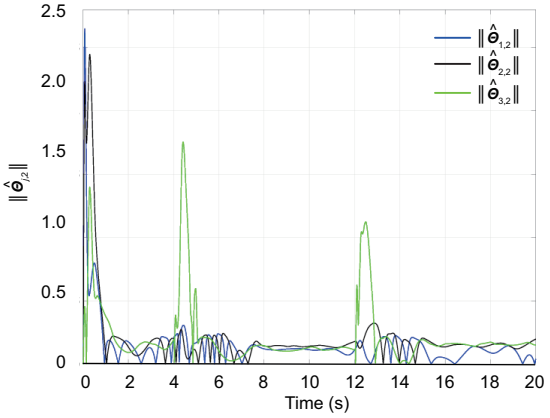

Fig. 4 Responses of the adaptive weights in Example 1

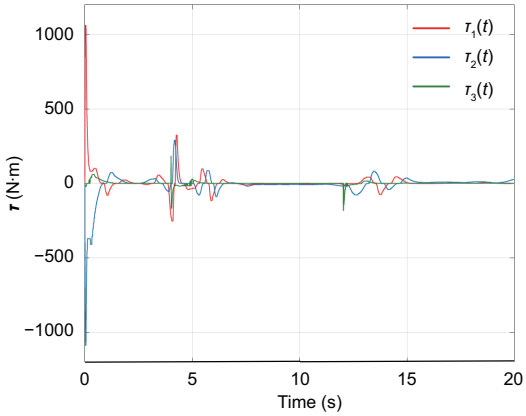

Fig. 5 Trajectories of control inputs in Example 1

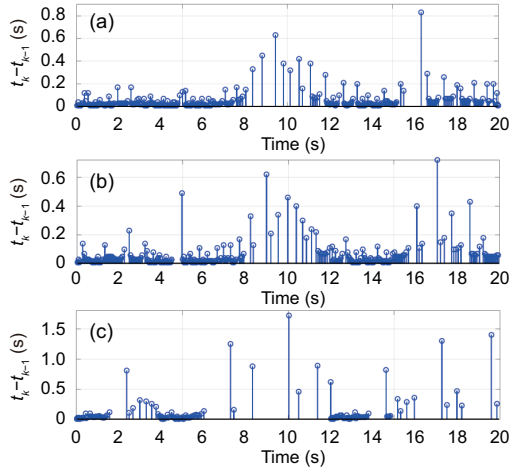

Fig. 6 Time intervals of triggering events $\tau_1(t)$ (a), $\tau_2(t)$ (b), and $\tau_3(t)$ (c) in Example 1

where $\boldsymbol{x}_1 = [x_{1,1}, x_{2,1}]^{\mathrm{T}}$ and $\boldsymbol{x}_2 = [x_{1,2}, x_{2,2}]^{\mathrm{T}}$ denote the joint position and velocity vectors, respectively, $\boldsymbol{D}(\boldsymbol{x}_1)$ denotes the inertia matrix, $\boldsymbol{C}(\boldsymbol{x}_1, \boldsymbol{x}_2)$ denotes the centripetal-Coriolis matrix, $\boldsymbol{G}(\boldsymbol{x}_1)$ denotes the gravity vector, and $\boldsymbol{F}(\boldsymbol{x}_1, \boldsymbol{x}_2, t)$ denotes the unmodeled structure vector. We define $\boldsymbol{F}_2(\boldsymbol{x}_1, \boldsymbol{x}_2) = \boldsymbol{D}^{-1}(\boldsymbol{x}_1)[-\boldsymbol{C}(\boldsymbol{x}_1, \boldsymbol{x}_2)\boldsymbol{x}_2 - \boldsymbol{G}(\boldsymbol{x}_1) - \boldsymbol{F}(\boldsymbol{x}_1, \boldsymbol{x}_2, t)]$. In this simulation, the function $\boldsymbol{F}_2(\boldsymbol{x}_1, \boldsymbol{x}_2)$ is assumed to be unknown. The detailed model information and values of the parameters in Eq. (81) can be found in Jin (2016).

The control parameters are selected as $k_1 = k_2 = 4$, $\sigma_1 = 0.1$, $\imath = \frac{5}{7}$, $\epsilon_1 = \epsilon_2 = 0.1$, $d = 0.1$, $\eta = 0.3$, and $\hbar = 5$. The parameters of the adaptive weights are given as $\gamma_2 = 1$ and $\kappa_2 = 10$. The simulation time is $t = 20$ s. The initial states are $\boldsymbol{x}_1(0) = [0,\ 1]^{\mathrm{T}}$ and $\boldsymbol{x}_2(0) = [0,\ 0]^{\mathrm{T}}$. Other initial values are given as zero. The desired trajectory is set as $\boldsymbol{y}_{\mathrm{d}} = [1 + \sin\left(\frac{\pi t}{4}\right), 1 - \cos\left(\frac{\pi t}{4}\right)]^{\mathrm{T}}$. The state constraints are selected as $\bar{\boldsymbol{b}}_1 = [4 + \sin\left(\frac{\pi t}{3}\right), 4 + \cos\left(\frac{\pi t}{3}\right)]^{\mathrm{T}}$, $\underline{\boldsymbol{b}}_1 = [2 + \sin t, 2 + \cos t]^{\mathrm{T}}$, $\bar{\boldsymbol{b}}_2 = [4 + \sin(2t), 4 + \sin(2t)]^{\mathrm{T}}$, and $\underline{\boldsymbol{b}}_2 = [4 + \sin(2t), 4 + \cos(2t)]^{\mathrm{T}}$. The fuzzy membership functions are the same as those in Example 1.

The simulation results are plotted in Figs. 7–10. The output-tracking performance under asymmetric time-varying state constraints is plotted in Fig. 7. Fig. 8 shows the system states under constraints. The ETC control law $\boldsymbol{\tau}(t)$ is shown in Fig. 9. The time intervals are plotted in Fig. 10. We can see from Fig. 7 that the system outputs can follow the reference trajectories well. As observed in Figs. 7 and 8, the proposed control approach can be easily applied

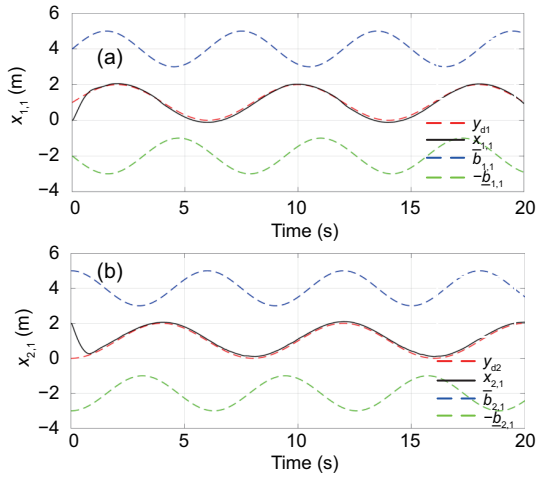

Fig. 7 Position-tracking performance under constraints $x_{1,1}$ (a) and $x_{2,1}$ (b) in Example 2

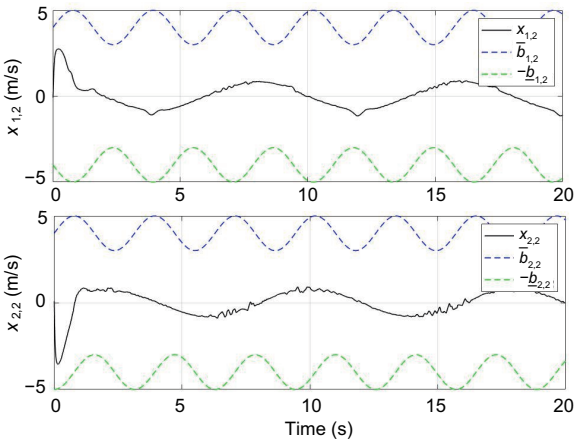

Fig. 8 Trajectories of the system states under constraints $x_{1,2}$ (a) and $x_{2,2}$ (b) in Example 2

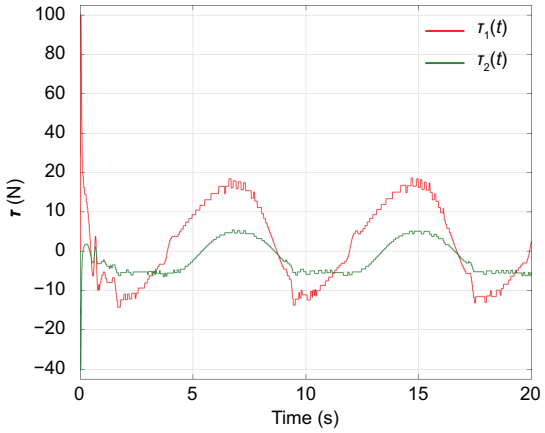

Fig. 9 Trajectories of control inputs in Example 2

to cope with the asymmetric time-varying state constraints. In Fig. 10, for τ_1 and τ_2, the total numbers of triggers are 337 and 329 respectively, and the numbers of non-triggering events are 1663 and 1671 respectively. Thus, using the designed ETC rule, the communication burden can be reduced significantly.

6 Conclusions

This paper investigated the issue of event-triggered adaptive finite-time control for MIMO nonlinear systems subject to asymmetric time-varying state constraints. With the help of tan-type NM, the considered system can be transformed into an equivalent "non-constrained" one, and the feasibility conditions can be removed. Based on the transformed system and the smooth switch function, a new adaptive fuzzy finite-time constrained-control approach was presented. Furthermore, the energy consumption was reduced using the designed ETC.

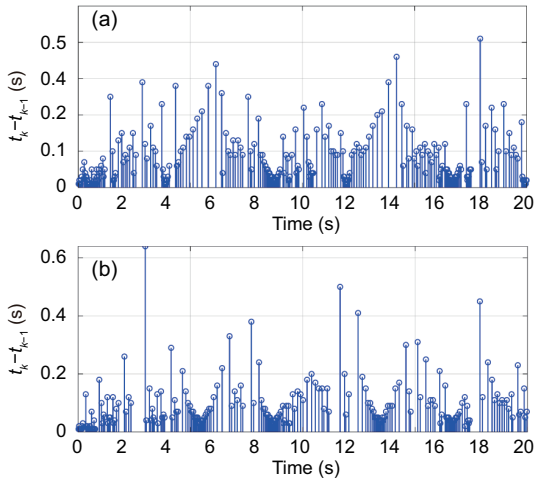

Fig. 10 Time intervals of triggering events $\tau_1(t)$ (a) and $\tau_2(t)$ (b) in Example 2

Stability analysis and two simulation examples were offered to confirm the effectiveness of the proposed ETC scheme. Our future works will expand this result to stochastic switched systems.

Contributors

Yan WEI designed the research. Jun LUO processed the data. Huaicheng YAN drafted the manuscript. Yueying WANG helped organize the manuscript. Yan WEI and Yueying WANG revised and finalized the paper.

Compliance with ethics guidelines

Yan WEI, Jun LUO, Huaicheng YAN, and Yueying WANG declare that they have no conflict of interest.

References

Chen CLP, Liu YJ, Wen GX, 2014. Fuzzy neural network-based adaptive control for a class of uncertain nonlinear stochastic systems. *IEEE Trans Cybern*, 44(5):583-593. https://doi.org/10.1109/TCYB.2013.2262935

Chen MH, Sun J, Karimi HR, 2020. Input-output finite-time generalized dissipative filter of discrete time-varying systems with quantization and adaptive event-triggered mechanism. *IEEE Trans Cybern*, 50(12):5061-5073. https://doi.org/10.1109/TCYB.2019.2932677

Cui B, Xia YQ, Liu K, et al., 2020. Finite-time tracking control for a class of uncertain strict-feedback nonlinear systems with state constraints: a smooth control approach. *IEEE Trans Neur Netw Learn Syst*, 31(11):4920-4932. https://doi.org/10.1109/TNNLS.2019.2959016

Cui RX, Yang CG, Li Y, et al., 2017. Adaptive neural network control of AUVs with control input nonlinearities using reinforcement learning. *IEEE Trans Syst Man Cybern Syst*, 47(6):1019-1029. https://doi.org/10.1109/TSMC.2016.2645699

Demirel B, Leong AS, Gupta V, et al., 2019. Tradeoffs in stochastic event-triggered control. *IEEE Trans Autom Contr*, 64(6):2567-2574. https://doi.org/10.1109/TAC.2018.2872199

Dong WJ, Farrell JA, Polycarpou MM, et al., 2012. Command filtered adaptive backstepping. *IEEE Trans Contr Syst Technol*, 20(3):566-580. https://doi.org/10.1109/TCST.2011.2121907

Ge SS, Wang C, 2004. Adaptive neural control of uncertain MIMO nonlinear systems. *IEEE Trans Neur Netw*, 15(3):674-692. https://doi.org/10.1109/TNN.2004.826130

Guo T, Wu XW, 2014. Backstepping control for output-constrained nonlinear systems based on nonlinear mapping. *Neur Comput Appl*, 25(7-8):1665-1674. https://doi.org/10.1007/s00521-014-1650-9

Hardy GH, Littlewood JE, Polya G, 1952. Inequalities. Cambridge University Press, Cambridge, UK.

Hua Y, Zhang TP, 2020a. Adaptive control of pure-feedback nonlinear systems with full-state time-varying constraints and unmodeled dynamics. *Int J Adapt Contr Signal Process*, 34(2):183-198. https://doi.org/10.1002/acs.3077

Hua Y, Zhang TP, 2020b. Adaptive neural event-triggered control of MIMO pure-feedback systems with asymmetric output constraints and unmodeled dynamics. *IEEE Access*, 8:37684-37696. https://doi.org/10.1109/ACCESS.2020.2975618

Jin X, 2016. Adaptive fault tolerant control for a class of input and state constrained MIMO nonlinear systems. *Int J Robust Nonlin Contr*, 26(2):286-302. https://doi.org/10.1002/rnc.3312

Li BW, Liu Y, Kou KI, et al., 2018. Event-triggered control for the disturbance decoupling problem of Boolean control networks. *IEEE Trans Cybern*, 48(9):2764-2769. https://doi.org/10.1109/TCYB.2017.2746102

Li GJ, 2017. Adaptive tracking control for air-breathing hypersonic vehicles with state constraints. *Front Inform Technol Electron Eng*, 18(5):599-614. https://doi.org/10.1631/FITEE.1500464

Li YM, Li KW, Tong SC, 2019. Finite-time adaptive fuzzy output feedback dynamic surface control for MIMO nonstrict feedback systems. *IEEE Trans Fuzzy Syst*, 27(1):96-110. https://doi.org/10.1109/TFUZZ.2018.2868898

Liu TF, Jiang ZP, 2015. A small-gain approach to robust event-triggered control of nonlinear systems. *IEEE Trans Autom Contr*, 60(8):2072-2085. https://doi.org/10.1109/TAC.2015.2396645

Liu Y, Jiang BX, Lu JQ, et al., 2020. Event-triggered sliding mode control for attitude stabilization of a rigid spacecraft. *IEEE Trans Syst Man Cybern Syst*, 50(9):3290-3299. https://doi.org/10.1109/TSMC.2018.2867061

Liu YJ, Ma L, Liu L, et al., 2020. Adaptive neural network learning controller design for a class of nonlinear systems with time-varying state constraints. *IEEE Trans Neur Netw Learn Syst*, 31(1):66-75. https://doi.org/10.1109/TNNLS.2019.2899589

Liu YL, Ma HJ, Ma H, 2018. Adaptive fuzzy fault-tolerant control for uncertain nonlinear switched stochastic systems with time-varying output constraints. *IEEE Trans Fuzzy Syst*, 26(5):2487-2498. https://doi.org/10.1109/TFUZZ.2018.2814596

Miao P, Shen YJ, Li YJ, et al., 2016. Finite-time recurrent neural networks for solving nonlinear optimization problems and their application. *Neurocomputing*, 177:120-129. https://doi.org/10.1016/j.neucom.2015.11.014

Polycarpou MM, 1996. Stable adaptive neural control scheme for nonlinear systems. *IEEE Trans Autom Contr*, 41(3):447-451. https://doi.org/10.1109/9.486648

Qian CJ, Lin W, 2001. Non-Lipschitz continuous stabilizers for nonlinear systems with uncontrollable unstable linearization. *Syst Contr Lett*, 42(3):185-200. https://doi.org/10.1016/S0167-6911(00)00089-X

Qiu JB, Sun KK, Rudas IJ, et al., 2020. Command filter-based adaptive NN control for MIMO nonlinear systems with full-state constraints and actuator hysteresis. *IEEE Trans Cybern*, 50(7):2905-2915. https://doi.org/10.1109/TCYB.2019.2944761

Sahoo A, Xu H, Jagannathan S, 2016. Neural network-based event-triggered state feedback control of nonlinear continuous-time systems. *IEEE Trans Neur Netw Learn Syst*, 27(3):497-509. https://doi.org/10.1109/TNNLS.2015.2416259

Swaroop D, Hedrick JK, Yip PP, et al., 2000. Dynamic surface control for a class of nonlinear systems. *IEEE Trans Autom Contr*, 45(10):1893-1899. https://doi.org/10.1109/TAC.2000.880994

Tee KP, Ge SS, 2011. Control of nonlinear systems with partial state constraints using a barrier Lyapunov function. *Int J Contr*, 84(12):2008-2023. https://doi.org/10.1080/00207179.2011.631192

Tee KP, Ge SS, 2012. Control of state-constrained nonlinear systems using integral barrier Lyapunov functionals. 51st IEEE Conf on Decision and Control, p.3239-3244. https://doi.org/10.1109/CDC.2012.6426196

Tee KP, Ge SS, Tay EH, 2009. Barrier Lyapunov functions for the control of output-constrained nonlinear systems. *Automatica*, 45(4):918-927. https://doi.org/10.1016/j.automatica.2008.11.017

Tian QY, Wei JH, Fang JH, et al., 2016. Adaptive fuzzy integral sliding mode velocity control for the cutting system of a trench cutter. *Front Inform Technol Electron Eng*, 17(1):55-66. https://doi.org/10.1631/FITEE.15a0160

Tong SC, Li YM, Shi P, 2012. Observer-based adaptive fuzzy backstepping output feedback control of uncertain MIMO pure-feedback nonlinear systems. *IEEE Trans Fuzzy Syst*, 20(4):771-785. https://doi.org/10.1109/TFUZZ.2012.2183604

Wang F, Chen B, Liu XP, et al., 2018. Finite-time adaptive fuzzy tracking control design for nonlinear systems. *IEEE Trans Fuzzy Syst*, 26(3):1207-1216. https://doi.org/10.1109/TFUZZ.2017.2717804

Wang LJ, Chen CLP, Li HY, 2020. Event-triggered adaptive control of saturated nonlinear systems with time-varying partial state constraints. *IEEE Trans Cybern*, 50(4):1485-1497. https://doi.org/10.1109/TCYB.2018.2865499

Wang M, Zhang SY, Chen B, et al., 2010. Direct adaptive neural control for stabilization of nonlinear time-delay systems. *Sci China Inform Sci*, 53(4):800-812. https://doi.org/10.1007/s11432-010-0075-z

Wang YC, Zheng WX, Zhang HG, 2017. Dynamic event-based control of nonlinear stochastic systems. *IEEE Trans Autom Contr*, 62(12):6544-6551. https://doi.org/10.1109/TAC.2017.2707520

Wang YC, Zhang JX, Zhang HG, et al., 2020. Adaptive fuzzy output-constrained control for nonlinear stochastic systems with input delay and unknown control coefficients. *IEEE Trans Cybern*, early access. https://doi.org/10.1109/TCYB.2020.3034146

Wang YY, Xia YQ, Ahn CK, et al., 2019. Exponential stabilization of Takagi-Sugeno fuzzy systems with aperiodic sampling: an aperiodic adaptive event-triggered method. *IEEE Trans Syst Man Cybern Syst*, 49(2):444-454. https://doi.org/10.1109/TSMC.2018.2834967

Wei Y, Zhou PF, Wang YY, et al., 2019. Adaptive neural dynamic surface control of MIMO uncertain nonlinear systems with time-varying full state constraints and disturbances. *Neurocomputing*, 364:16-31. https://doi.org/10.1016/j.neucom.2019.07.033

Wei Y, Zhou PF, Liang YZ, et al., 2020a. Adaptive finite-time neural backstepping control for multi-input and multi-output state-constrained nonlinear systems using tangent-type nonlinear mapping. *Int J Robust Nonlin Contr*, 30(14):5559-5578. https://doi.org/10.1002/rnc.5096

Wei Y, Wang YY, Ahn CK, et al., 2020b. IBLF-based finite-time adaptive fuzzy output-feedback control for uncertain MIMO nonlinear state-constrained systems. *IEEE Trans Fuzzy Syst*, early access. https://doi.org/10.1109/TFUZZ.2020.3021733

Xia JW, Zhang J, Sun W, et al., 2019. Finite-time adaptive fuzzy control for nonlinear systems with full state constraints. *IEEE Trans Syst Man Cybern Syst*, 49(7):1541-1548. https://doi.org/10.1109/TSMC.2018.2854770

Xing LT, Wen CY, Liu ZT, et al., 2017. Event-triggered adaptive control for a class of uncertain nonlinear systems. *IEEE Trans Autom Contr*, 62(4):2071-2076. https://doi.org/10.1109/TAC.2016.2594204

Xing LT, Wen CY, Liu ZT, et al., 2019. Event-triggered output feedback control for a class of uncertain nonlinear systems. *IEEE Trans Autom Contr*, 64(1):290-297. https://doi.org/10.1109/TAC.2018.2823386

Xu T, Hao YQ, Duan ZS, 2020. Fully distributed containment control for multiple Euler-Lagrange systems over directed graphs: an event-triggered approach. *IEEE Trans Circ Syst I Reg Papers*, 67(6):2078-2090. https://doi.org/10.1109/TCSI.2020.2971037

Xue T, Wang ZW, Zhang T, et al., 2020. Fixed-time constrained acceleration reconstruction scheme for robotic exoskeleton via neural networks. *Front Inform Technol Electron Eng*, 21(5):705-722. https://doi.org/10.1631/FITEE.1900418

Yu JP, Shi P, Dong WJ, et al., 2015. Observer and command-filter-based adaptive fuzzy output feedback control of uncertain nonlinear systems. *IEEE Trans Ind Electron*, 62(9):5962-5970. https://doi.org/10.1109/TIE.2015.2418317

Yu JP, Yu H, Lin CS, et al., 2018. Fuzzy finite-time command filtered control of nonlinear systems with input saturation. *IEEE Trans Cybern*, 48(8):2378-2387. https://doi.org/10.1109/TCYB.2017.2738648

Zhang TP, Xia MZ, Yi Y, et al., 2017. Adaptive neural dynamic surface control of pure-feedback nonlinear systems with full state constraints and dynamic uncertainties. *IEEE Trans Syst Man Cybern Syst*, 47(8):2378-2387. https://doi.org/10.1109/TSMC.2017.2675540

Zhang TP, Liu HQ, Xia MZ, et al., 2018. Adaptive neural control of MIMO uncertain nonlinear systems with unmodeled dynamics and output constraint. *Int J Adapt Contr Signal Process*, 32(12):1731-1747. https://doi.org/10.1002/acs.2939

Zhao K, Song YD, 2019. Removing the feasibility conditions imposed on tracking control designs for state-constrained strict-feedback systems. *IEEE Trans Autom Contr*, 64(3):1265-1272. https://doi.org/10.1109/TAC.2018.2845707

Zhao K, Song YD, 2020. Neuroadaptive robotic control under time-varying asymmetric motion constraints: a feasibility-condition-free approach. *IEEE Trans Cybern*, 50(1):15-24. https://doi.org/10.1109/TCYB.2018.2856747

Zhu SY, Liu Y, Lou YJ, et al., 2020. Stabilization of logical control networks: an event-triggered control approach. *Sci China Inform Sci*, 63(1):112203. https://doi.org/10.1007/s11432-019-9898-3

Appendix A: Proof of Lemma 7

Using proof by contradiction: Suppose that some time $t = t_1$ and a constant $\Delta \geq 0$ exist, such that $x_{j,r_j}(t_1) = \bar{b}_{j,r_j} + \Delta$ or $x_{j,r_j}(t_1) = -\underline{b}_{j,r_j} - \Delta$. Because $x_{j,r_j}(t)$ is a continuous function, there exists a time instant $0 < t^* < t_1$ such that $x_{j,r_j}(t^*) = \bar{b}_{j,r_j}$ or $x_{j,r_j}(t^*) = -\underline{b}_{j,r_j}$. Then, we have $\varpi_{j,r_j}(t^*) = \xi_{j,r_j}(\bar{b}_{j,r_j}) = \infty$ or $\varpi_{j,r_j}(t^*) = \xi_{j,r_j}(-\underline{b}_{j,r_j}) = -\infty$, which leads to the boundedness of $\varpi_{j,r_j}(t)$. Because $x_{j,r_j}(0) \in \Omega_x$, we have $x_{j,r_j}(t) \in \Omega_x$, $\forall t \geq 0$. This completes the proof.

Appendix B: Proof of Lemma 8

According to Definition 2, we can determine that ξ and ξ^{-1} are two continuous functions. Define $\chi_{j,r_j}=\varpi_{j,r_j}-l^*$ and $e_{j,r_j}=x_{j,r_j}-l$. First, we assume that $x_{j,r_j}\geq 0$. Then, we have

$$\begin{aligned} e_{j,r_j} =&x_{j,r_j}-l\\ =&\frac{2\bar{b}_{j,r_j}}{\pi}\left[\arctan\left(\frac{\pi\varpi_{j,r_j}}{2\bar{b}_{j,r_j}}\right)-\arctan\left(\frac{\pi l^*}{2\bar{b}_{j,r_j}}\right)\right]\\ =&\frac{2\bar{b}_{j,r_j}}{\pi}\arctan\frac{\pi}{2\bar{b}_{j,r_j}}\left(\frac{\varpi_{j,r_j}-l^*}{1+\frac{\pi^2\varpi_{j,r_j}l^*}{4\bar{b}^2_{j,r_j}}}\right). \end{aligned} \tag{B1}$$

From Eq. (B1), we can obtain

$$\begin{aligned} &\lim_{e_{j,r_j}\to 0}e_{j,r_j}\\ &\quad=\lim_{\varpi_{j,r_j}\to l^*}\frac{2\bar{b}_{j,r_j}}{\pi}\arctan\frac{\pi}{2\bar{b}_{j,r_j}}\left(\frac{\varpi_{j,r_j}-l^*}{1+\frac{\pi^2\varpi_{j,r_j}l^*}{4\bar{b}^2_{j,r_j}}}\right)\\ &\quad=0. \end{aligned} \tag{B2}$$

Thus, we have $\varpi_{j,r_j}\to l^*$ as $x_{j,r_j}\to l$. For $x_{j,r_j}<0$, the proof process is the same as that in the case of $x_{j,r_j}\geq 0$.